Supporting Information

Light-activated Inorganic $CsPbBr_2I$ Perovskite for Room-Temperature Self-Powered Chemical Sensing

Hongjun Chen, Meng Zhang, Xiao Fu, Zelio Fusco, Renheng Bo, Bobo Xing, Hieu T. Nguyen, Chog Barugkin, Jianghui Zheng, Cho Fai Jonathan Lau, Shujuan Huang, Anita W. Y. Ho-Baillie, Kylie R. Catchpole and Antonio Tricoli**

Dr. H. Chen, Z. Fusco, R. Bo, B. Xing, Prof. A. Tricoli
Nanotechnology Research Laboratory, Research School of Electrical, Energy and Materials Engineering, College of Engineering and Computer Sciences, Australian National University, Canberra 2601, Australia
E-mail: antonio.tricoli@anu.edu.au; hongjun.chen@anu.edu.au
Dr. M. Zhang, J. Zheng, C. F. J. Lau, Dr. S. Huang, Assoc. Prof. A. W. Y. Ho-Baillie, Australian Centre for Advanced Photovoltaics, School of Photovoltaic and Renewable Energy Engineering, University of New South Wales, Sydney 2052, Australia
X. Fu, Dr. H. T. Nguyen, Dr. C. Barugkin, Prof. K. R. Catchpole
Research School of Electrical, Energy and Materials Engineering, College of Engineering and Computer Sciences, Australian National University, Canberra 2601, Australia

Keywords: Inorganic halides perovskites, chemical sensors, trap states, self-powered, volatile organic compounds

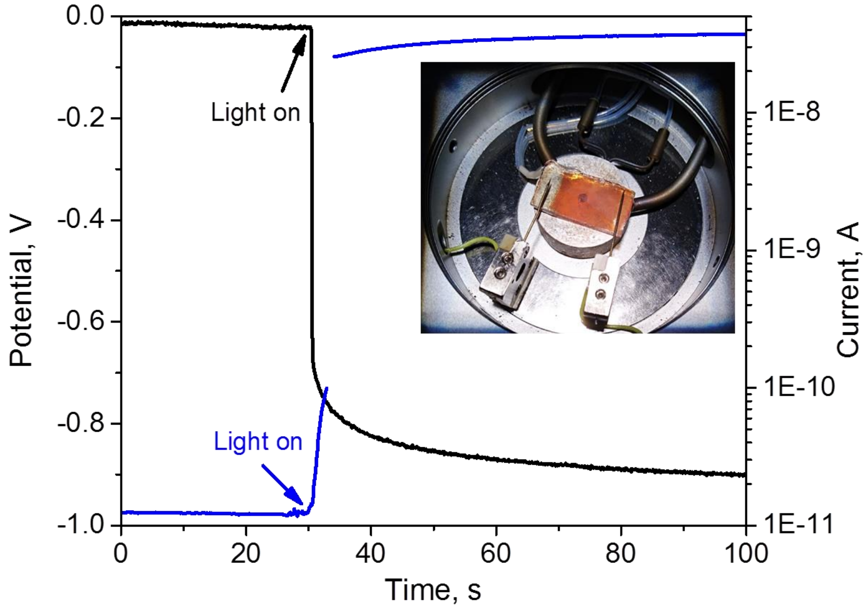

Fig. S1. The open circuit potential (black line) and short-circuit current (blue line) of CPBI devices in dark and simulated solar irradiation, the inset is the picture of the CPBI device with the top contact. The measurements were conducted under simulated air atmosphere. The broken blue line is due to changing the current scale.

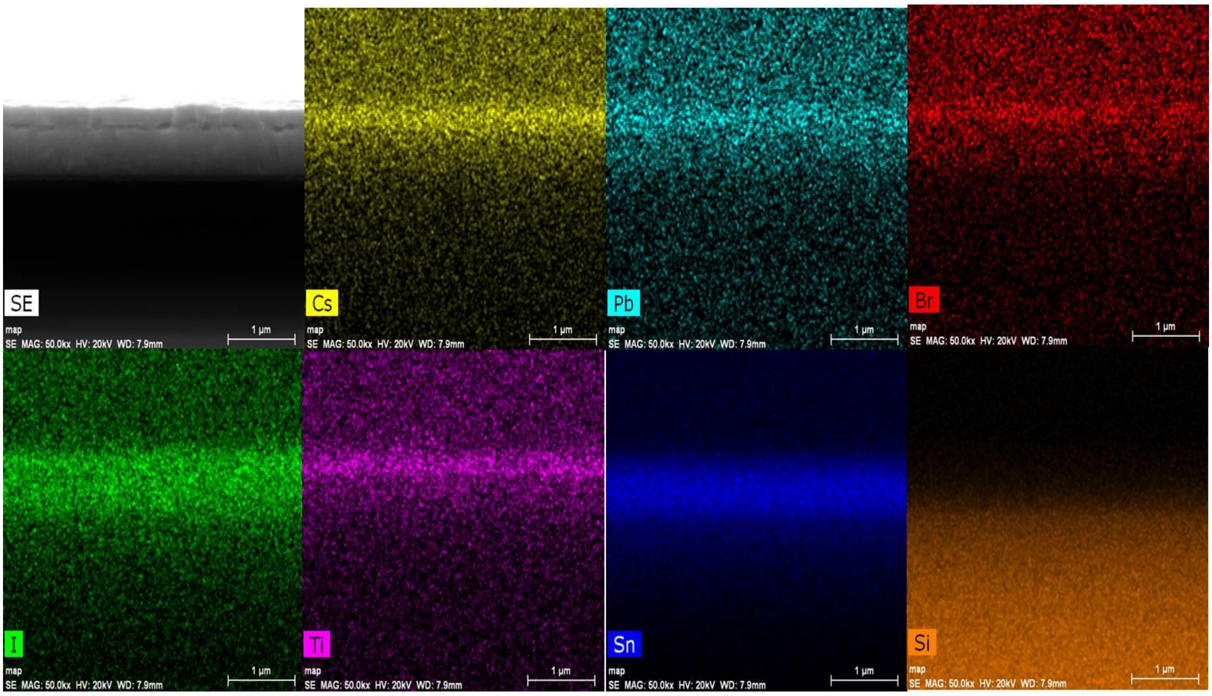

Fig. S2. EDS mapping of various elements distributed within the cross-section of CPBI film on a compact TiO_2 layer on a FTO glass substrate, the scale bar is 1 micrometre.

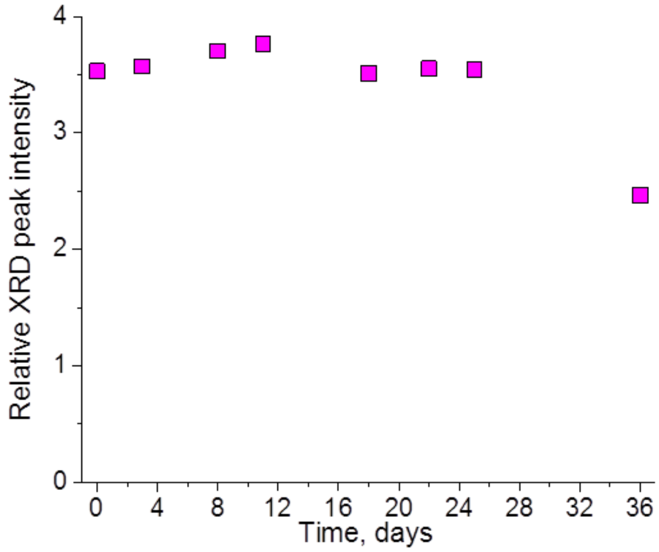

Fig. S3. The structural stability of CPBI devices with different storage time. The relative XRD peak intensity was calculated based on the ratio between the (100) peak of CPBI located at 2θ of 15.2 ^{o} and the main peak of FTO located at 2θ of 26.5 ^{o}.

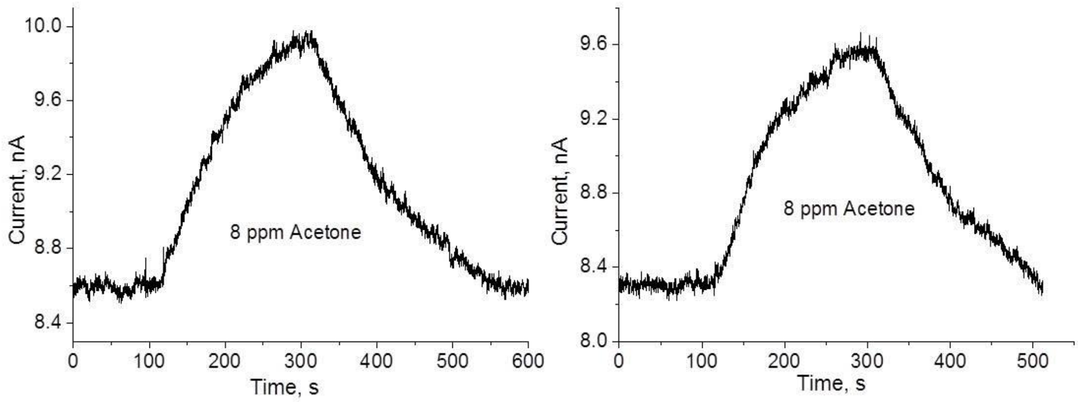

Fig. S4. Photocurrent response kinetics of two different batches of CPBI sensors to injection of 8 ppm of acetone in pure N_2.

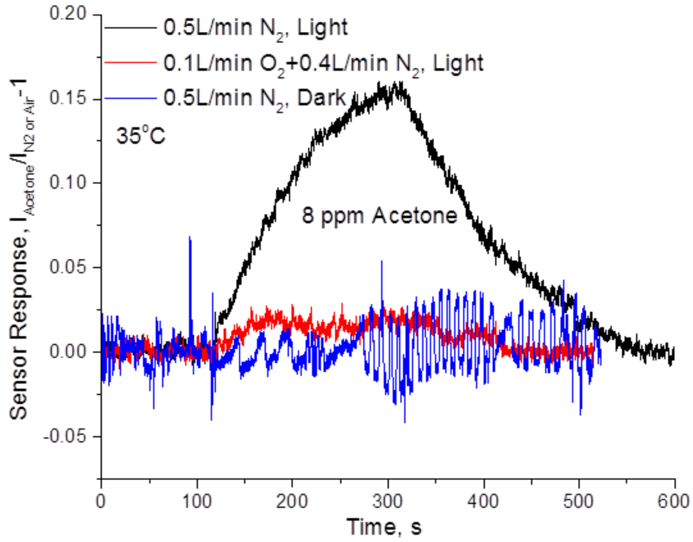

Fig. S5. Dynamic CPBI sensor response to injection of 8 ppm of acetone in pure N_2 (black line) and simulated air (red line) under simulated solar irradiation (AM 1.5, 42.3 mWcm^{-2}), and in pure N_2 under dark (blue line). Due to the tiny current under dark (~ 0.13 nA), the sensor response of CPBI in pure N_2 under dark is quite noisy.

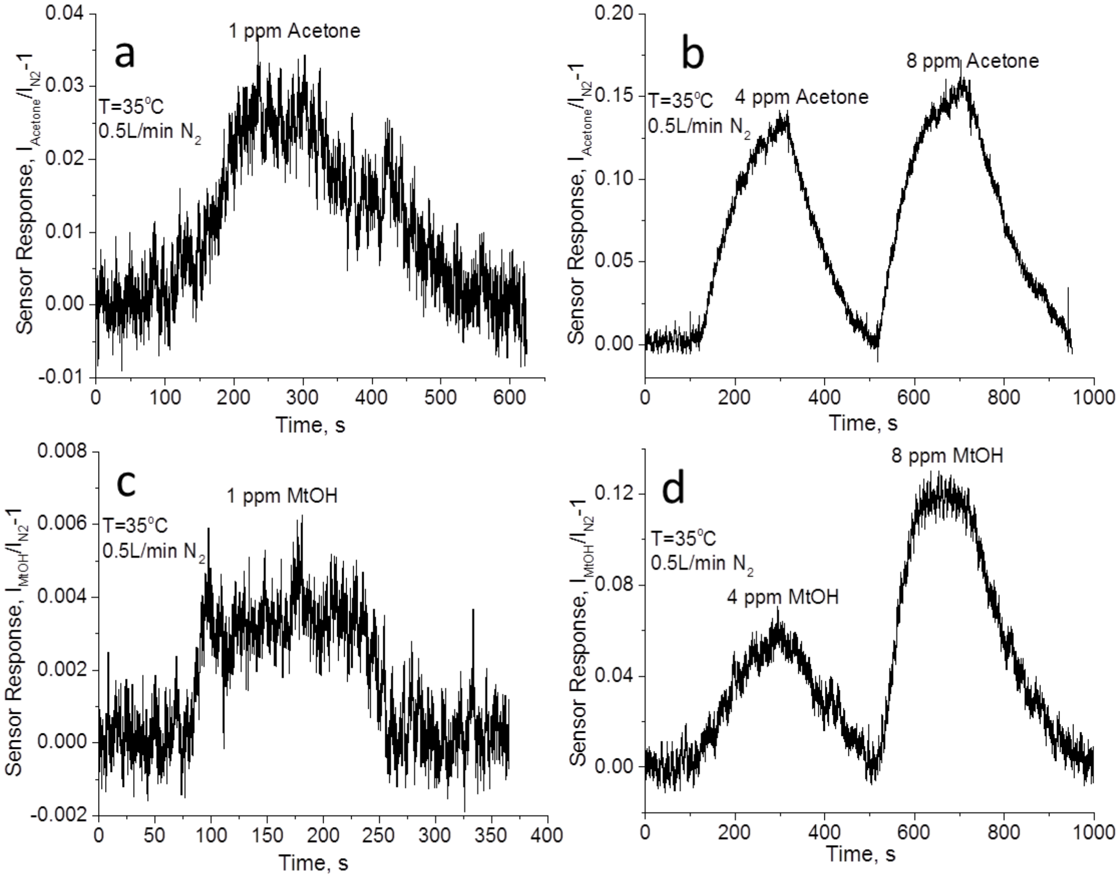

Fig. S6. Dynamic CPBI sensor response to injection of 1 ppm (a and c), 4 and 8 ppm (b and d) of acetone (a and b) and methanol (c and d) in pure N_2 atmosphere under simulated solar irradiation (AM 1.5, 42.3 $mWcm^{-2}$). Due to the switch of mass flow controllers with different gas flow rate ranges, the dynamic curve of CPBI sensor for the same gas with different concentrations are draw separately.

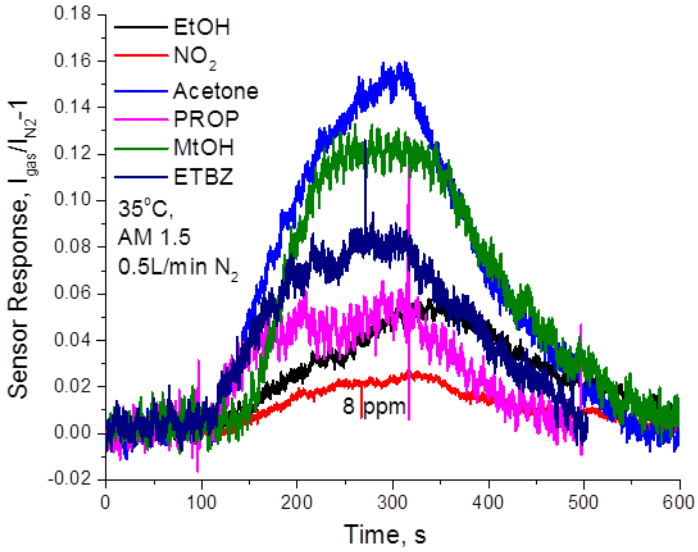

Fig. S7. Dynamic CPBI sensor response to injection of 8 ppm of five VOCs and one NO_2 gases in pure N_2 atmosphere under simulated solar irradiation (AM 1.5, 42.3 $mWcm^{-2}$).

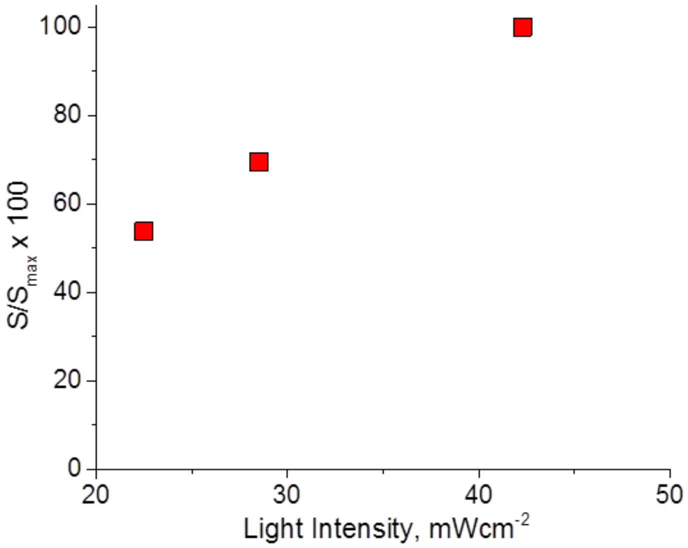

Fig. S8. The relationship between the sensor response and illumination light intensity.

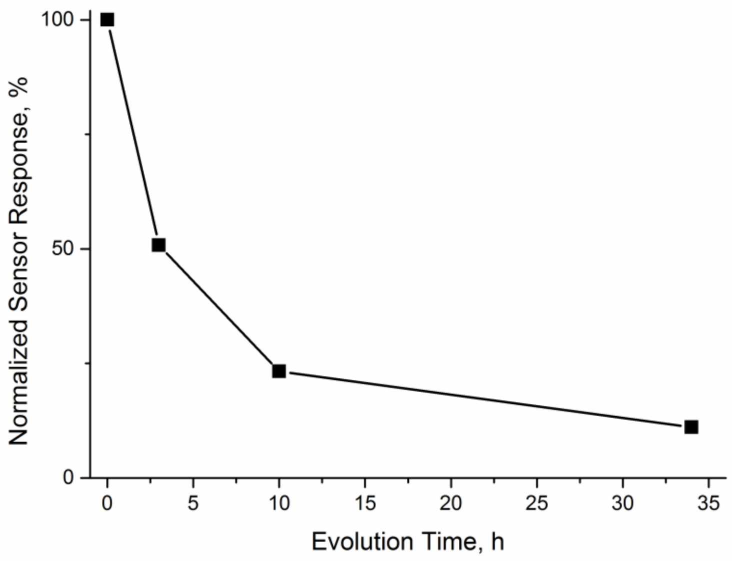

Fig. S9. The sensor response of the device as a function of evolution time under air with humidity around 20-35%.

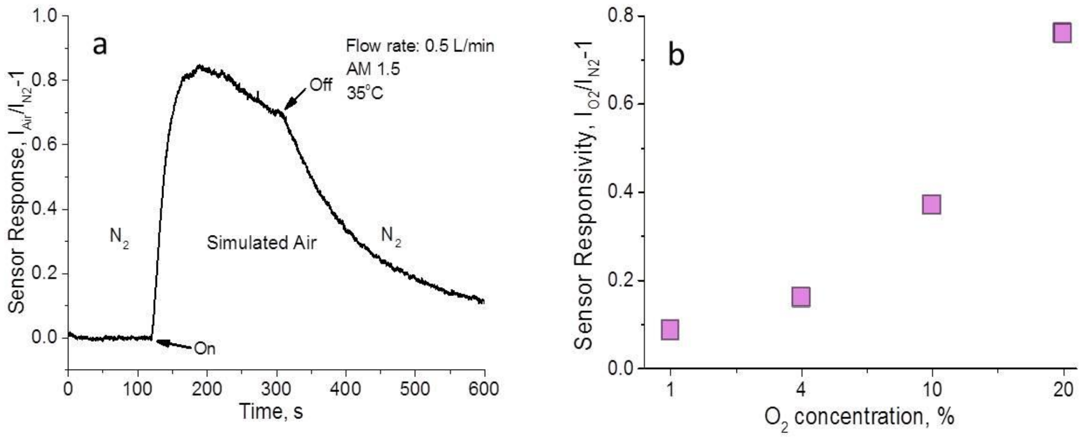

Fig. S10. Dynamic CPBI sensor response to different environmental atmospheres (0.5 L/min N_2 or 0.4 L/min N_2 + 0.1 L/min O_2) under simulated solar irradiation (AM 1.5, 42.3 mWcm^{-2}) and the response time is ca. 34 s (the time to reach 90% of the maximum sensor response) (a), and CPBI sensor responsivity as function of the O_2 concentration in N_2 from 1% to 20 % (b).

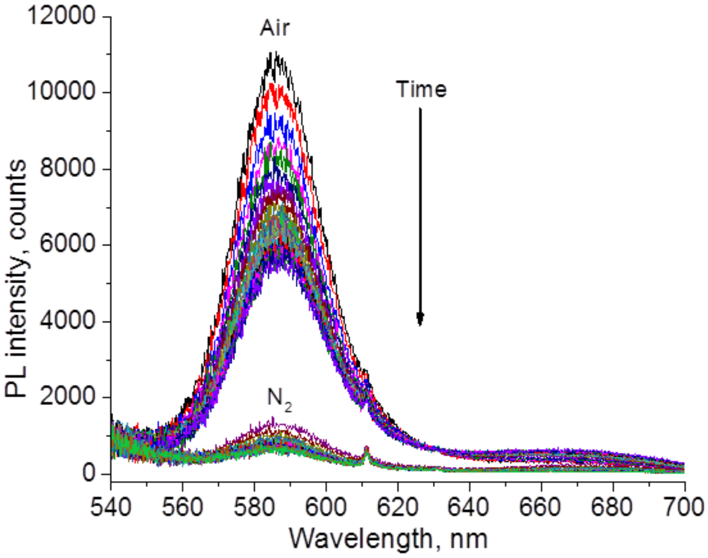

Fig. S11. The consecutive PL spectra of CPBI sensor under different environmental atmospheres.

Table S1. the summary of the state-of-art perovskite based and other photo- and chemoresistive sensors.

Material	Light	Bias	Response time	Analyte gas/LOD*	Ref.
$CsPbBr_2I$	Y	N	~ 100-150 s	Various VOCs / 1 ppm	This work
$CH_3NH_3PbI_{3-x}Cl_x$	Y	N	~ 188-225 s	O_3 / 5 ppb	1
$CsPbBr_3$	Y	N	~ 17-77 s	O_2 / 1% Acetone / 1 ppm; Ethanol / 1 ppm	2
$CH_3NH_3PbI_3$	N	Y/ 4 V	~400 ms	O_2 / 70 ppm	3
$CH_3NH_3PbI_{3-x}Cl_x$	N	Y/ 10 V	~1400 s	Moisture/32 %	4
$CH_3NH_3PbI_3$	N	Y/ 10 V	~22 s	NO_2 / 1 ppm	5
$CH_3NH_3PbI_3$	N	Y/ 1.5 V	~ 3 s	NH_3 / 33 %	6
$CH_3NH_3PbI_{3-x}(SCN)_x$	N	Y/ 1 V	~ 220-270 s	Acetone / 20 ppm; NO_2 / 200 ppb	7
p-Si/n-ZnO	Y	N	~ 1500 s	NO_2 / 250 ppb	8
CdS@n-ZnO/p-Si	Y	N	~ 1200 s	Ethanol / 50 ppm, methane / 50 ppm	9
NiO-ZnO nanoheterojunction networks	Y	Y / 1 V	~ 900 s	Various VOCs including ethanol, acetone, etc. / 1 ppm	10
Cobalt-doped ZnO (1%) nanobelts	Y	Y / 9.65 V	~ 90-120 s	Ethanol / 2.9 Torr	11
ZnO/Ag_2S heterogeneous microspheres	Y	Y / 9.65 V	~ 10 s	Ethanol / 50 ppm	12
porphyrin-functionalized ZnO nanorod	Y	Y / 1 V	~ 100 s	Ethanol / 8%; Triethylamine / 8%	13

LOD*, limit of detection;

Table S2. Room-temperature response time of various chemoresistive MOS sensors to VOCs.

Material	Response time	Analyte gas	Ref.
$CsPbBr_2I$	~ 2-3 min	various VOCs including ethanol, acetone, etc.	This work
NiO-ZnO nanoheterojunction networks	~ 15 min	various VOCs including ethanol, acetone, etc.	10
p-Si/n-ZnO	~ 25 min	NO_2	8
CdS@n-ZnO/p-Si	~ 20 min	O_2, ethanol, methane	9
WO_3	~ 25 min	NO_2	14
Nanoporous In_2O_3 particles	~ 25 min	ozone	15
Nanocrystalline ZnO sensitized with CdSe	~ 50 min	NO_2	16
cobalt-doped ZnO nanobelts	~ 10 min	Ethanol	11
ZnO nanorods/SnO_2 nanoparticles	~ 25 min	NO_2	17
polycrystalline ZnO	~ 15 min	H_2	18
ZnO nanorods	~ 13 min	Formaldehyde	19
quasi-2D Cu_2O/SnO_2	~ 10 min	H_2S	20
Nanopatterned polycrystalline ZnO	~ 13 min	H_2, NO_2	21
ZnO nanoparticles	~ 8.5 min	Ethanol	22
SnO_2 pyrolytic films	~ 10 min	acetone and trichloroethylene	23
Hollow TiO_2 microspheres	~ 8-10 min	formaldehyde	24
copper-doped ZnO	~ 10 min	ethanol and acetone	25
SnO_2 thin films	~ 2-3 min	various VOCs including ethanol, 2-pentanone, etc	26

References

1. G. Kakavelakis, E. Gagaoudakis, K. Petridis, V. Petromichelaki, V. Binas, G. Kiriakidis and E. Kymakis, *ACS Sens.*, 2018, **3**, 135-142.
2. H. Chen, M. Zhang, R. Bo, C. Barugkin, J. Zheng, Q. Ma, S. Huang, A. W. Y. Ho-Baillie, K. R. Catchpole and A. Tricoli, *Small*, DOI: 10.1002/smll.201702571, 1702571.
3. M.-A. Stoeckel, M. Gobbi, S. Bonacchi, F. Liscio, L. Ferlauto, E. Orgiu and P. Samorì, *Adv. Mater.*, 2017, **29**, 1702469.
4. L. Hu, G. Shao, T. Jiang, D. Li, X. Lv, H. Wang, X. Liu, H. Song, J. Tang and H. Liu, *ACS Appl. Mater. Interfaces*, 2015, **7**, 25113-25120.
5. X. Fu, S. Jiao, N. Dong, G. Lian, T. Zhao, S. Lv, Q. Wang and D. Cui, *RSC Adv.*, 2018, **8**, 390-395.
6. C. Bao, J. Yang, W. Zhu, X. Zhou, H. Gao, F. Li, G. Fu, T. Yu and Z. Zou, *Chem. Commun.*, 2015, **51**, 15426-15429.
7. Y. Zhuang, W. Yuan, L. Qian, S. Chen and G. Shi, *Phys. Chem. Chem. Phys.*, 2017, **19**, 12876-12881.
8. M. W. G. Hoffmann, L. Mayrhofer, O. Casals, L. Caccamo, F. Hernandez-Ramirez, G. Lilienkamp, W. Daum, M. Moseler, A. Waag, H. Shen and J. D. Prades, *Adv. Mater.*, 2014, **26**, 8017-8022.
9. M. W. G. Hoffmann, A. E. Gad, J. D. Prades, F. Hernandez-Ramirez, R. Fiz, H. Shen and S. Mathur, *Nano Energy*, 2013, **2**, 514-522.
10. H. Chen, R. Bo, A. Shrestha, B. Xin, N. Nasiri, J. Zhou, I. Di Bernardo, A. Dodd, M. Saunders, J. Lipton-Duffin, T. White, T. Tsuzuki and A. Tricoli, *Adv. Optical Mater.*, **0**, 1800677.
11. L. Peng, Q. Zeng, H. Song, P. Qin, M. Lei, B. Tie and T. Wang, *Appl. Phys. A*, 2011, **105**, 387-392.
12. Y. Zhang, B. Liu, D. Wang, Y. Lin, T. Xie and J. Zhai, *Mater. Chem. Phys.*, 2012, **133**, 834-838.
13. Y. Sivalingam, E. Martinelli, A. Catini, G. Magna, G. Pomarico, F. Basoli, R. Paolesse and C. Di Natale, *J. Phys. Chem. C*, 2012, **116**, 9151-9157.
14. C. Zhang, A. Boudiba, P. De Marco, R. Snyders, M.-G. Olivier and M. Debliquy, *Sens. Actuators, B*, 2013, **181**, 395-401.
15. D. Klaus, D. Klawinski, S. Amrehn, M. Tiemann and T. Wagner, *Sens. Actuators, B*, 2015, **217**, 181-185.
16. A. S. Chizhov, M. N. Rumyantseva, R. B. Vasiliev, D. G. Filatova, K. A. Drozdov, I. V. Krylov, A. M. Abakumov and A. M. Gaskov, *Sens. Actuators, B*, 2014, **205**, 305-312.
17. G. Lu, J. Xu, J. Sun, Y. Yu, Y. Zhang and F. Liu, *Sens. Actuators, B*, 2012, **162**, 82-88.
18. S.-W. Fan, A. K. Srivastava and V. P. Dravid, *Appl. Phys. Lett.*, 2009, **95**, 142106.
19. L. Peng, Q. Zhao, D. Wang, J. Zhai, P. Wang, S. Pang and T. Xie, *Sens. Actuators, B*, 2009, **136**, 80-85.
20. G. Cui, M. Zhang and G. Zou, *Sci. Rep.*, 2013, **3**, 1250.
21. S.-W. Fan, A. K. Srivastava and V. P. Dravid, *Sens. Actuators, B*, 2010, **144**, 159-163.
22. Z. Q. Zheng, J. D. Yao, B. Wang and G. W. Yang, *Sci. Rep.*, 2015, **5**, 11070.
23. J. Saura, *Sens. Actuators, B*, 1994, **17**, 211-214.
24. X. Li, X. Li, J. Wang and S. Lin, *Sens. Actuators, B*, 2015, **219**, 158-163.
25. L. Peng, T.-F. Xie, M. Yang, P. Wang, D. Xu, S. Pang and D.-J. Wang, *Sens. Actuators, B*, 2008, **131**, 660-664.
26. K. Haddad, A. Abokifa, S. Kavadiya, B. Lee, S. Banerjee, B. Raman, P. Banerjee, C. Lo, J. Fortner and P. Biswas, *ACS Appl. Mater. Interfaces*, 2018, **10**, 29972-29981.